Surface ozone climatology of South Eastern Brazil and the impact of biomass burning events

Targino, Admir Créso; Harrison, Roy M.; Krecl, Patricia; Glantz, Paul; de Lima, Caroline Hatada; Beddows, David

DOI:
10.1016/j.jenvman.2019.109645

Surface ozone climatology of South Eastern Brazil and the impact of biomass burning events

Admir Créso Targino[a,†,*], Roy M. Harrison [b,††], Patricia Krecl[a], Paul Glantz[c]
Caroline Hatada de Lima[a,†], David Beddows[b]

[a]Graduate Program in Environmental Engineering, Federal University of Technology, Av. Pioneiros 3131, 86036-370, Londrina, PR, Brazil

[b]School of Geography, Earth and Environmental Sciences, University of Birmingham, Edgbaston, Birmingham, B15 2TT, United Kingdom

[c]Department of Environmental Science and Analytical Chemistry, Stockholm University, Svante Arrhenius väg 8, 106 91, Stockholm, Sweden

[†]Also at: Graduate Program in Geography, Londrina State University, Rod. Celso Garcia, Km 380, 86057-970, Londrina, PR, Brazil

[††] Also at: Department of Environmental Sciences, Centre of Excellence in Environmental Studies, King Abdulaziz University, PO Box 80203, Jeddah, 21589, Saudi Arabia.

*Corresponding author: admirtargino@utfpr.edu.br

Abstract

In the austral spring, biomass fires affect a vast area of South America each year. We combined *in situ* ozone (O_3) data, measured in the states of São Paulo and Paraná, Brazil, in the period 2014-2017, with aerosol optical depth, co-pollutants (NOx, $PM_{2.5}$ and PM_{10}) and air backtrajectories to identify sources, transport and geographical patterns in the air pollution data. We applied cluster analysis to hourly O_3 data and split the investigation area of approximately 290,000 km^2 into five groups with similar features in terms of diurnal, weekly, monthly and seasonal O_3 concentrations. All groups presented a peak in September and October, associated with the fire activities and enhanced photochemistry. The highest mean O_3 concentrations were measured inland whilst, besides having lower concentrations, the coastal group was also associated with the smallest diurnal and seasonal variations. The latter was attributed to lower photochemical activity due to frequently occurring overcast weather situation. The mean annual regional contribution of O_3 over the area was 61 $\mu g/m^3$, with large seasonal and intersite variabilities (from 35 to 84 $\mu g/m^3$). The long-range transport of smoke contributed with between 23 and 41% of the total O_3 during the pollution events. A pollution outbreak in September 2015 caused many-fold increases in O_3, $PM_{2.5}$ and PM_{10} across the investigation area, which exceeded the World Health Organisation recommendations. We show that the regional transport of particulates and gas due to biomass burning overlays the local emissions in already highly polluted cities. Such an effect can outweigh local measures to curb anthropogenic air pollution in cities.

Key words: Short-lived climate forcer; Transboundary pollution; Cluster analysis; Air quality

1. Introduction

Planet Earth is frequently affected by smoke from fires caused by humans (*e.g.*, burning of vegetation and waste, preparation of agriculture fields, conversion of cropland to pasture) and by natural processes (*e.g.*, lightning-induced fires). Australia, California and many other regions of Earth are prone to wildfires, defined as uncontrollable fires caused by the concomitant occurrence of vegetative resources to burn (such as forest, shrub or grass), sustained dry spells and ignition sources. Wildfires are seasonal because the constraints for their occurrence (especially fire-conducive weather patterns) occur in specific periods of the year (Krawchuk *et al*., 2009). Fires that particularly take place at low temperatures and limited oxygen favour the formation of trace gases, such as VOC, CO and NOx ($NO+NO_2$), and particulate matter ($PM_{2.5}$, PM_{10} and black carbon) (Akagi *et al*., 2011; Wevers *et al.*, 2004; Crutzen and Andreae, 1990). The transboundary transport of smoke from wildfires and agricultural burns deteriorates the air quality downstream of the burning areas (McClure and Jaffe, 2018a; Targino and Krecl, 2016; Sarangi *et al*., 2014; Sillanpää *et al.*, 2005), even at a considerable distances from the sources (over 2,000 km, see Targino *et al.*, 2013 and Witham and Manning, 2007).

One aggravating aspect about wildfires is that they are becoming longer and more frequent in some regions of the planet, such as Eurasia and western North America (Riaño *et al.*, 2007), which may be related to anthropogenic climate change (Flannigan *et al.*, 2013; 2009). For South America, Riaño *et al.* (2007) showed a consistent fire regime of interannual cycles with no clear trends for any month or annually. The majority of wildfires in Brazil occurs in the dry season (between July and September) in the areas of Amazon, Cerrado (a savanna-like biome of central Brazil) and in the Pampas (grasslands in Southern Brazil). In the Amazon and Cerrado, the wildfires are predominantly man-made, with the purpose of removing brush, accumulated waste and vegetation to install

crop cultures or pastures (Ten Hoeve *et al.*, 2012; Pivello, 2011). Moreover, sugar cane field burning to eliminate the sharp-edged leaves and poisonous animals before harvesting also contributes to regional biomass smoke (Allen *et al.*, 2004).

Depending on the meteorological setting, the long-range transport of smoke during the dry season affects the air quality of small and large cities downwind of the fire spots, including the megacity of São Paulo (e.g., Lopes *et al.*, 2012; Freitas *et al.*, 2005; Reinhardt, 2001). Freitas *et al.* (2005) observed that the position of the South Atlantic subtropical high pressure plays an important role in the transport of aerosol plumes from the Amazon region to Southern Brazil. This system also prevents rain-bearing cold fronts from penetrating the area, favouring the accumulation of pollutants and deterioration of the air quality (Oliveira *et al.*, 2016; Targino and Krecl, 2016).

The hotspot of primary pollutants is found at the fire front, whilst high concentrations of secondary pollutants, such as tropospheric ozone (O_3) are usually detected a few kilometres downwind of the burning area (Wentworth *et al.*, 2018). O_3 is formed via a series of complex, non-linear reactions involving NOx and non-methane VOC in the presence of sunlight (Monks *et al.*, 2015 and references therein). The O_3 production rate is governed by NOx- or VOC-limited conditions and possibly aerosol effects on the photochemical production (Baylon *et al.*, 2018; Alvarado *et al.*, 2015).

Many countries have targeted the transportation sector as a strategy for abating air pollution and global warming. For example, in 2015, the mayors of eight Latin American cities (Curitiba, Rio de Janeiro, Salvador, Bogotá, Quito, Caracas, Buenos Aires and Mexico City) members of C40 –a network of the world's megacities committed to tackle climate change (www.c40.org)– signed a declaration of intent in which 35% of the diesel-fuelled public buses will be replaced by hybrid and electric buses by 2020. Although this is an important measure to tackle air pollution in cities, they may not be enough if other

97 sources prevail, such as biomass burning. McClure and Jaffe (2018a) reported maximum
98 daily (8-h average) O_3 increase up to 70 μg/m^3 on days affected by smoke in Meridian
99 (USA). Zhou *et al.* (2019) observed a concomitant 2.5-fold increase in O_3 concentrations
100 at three sites in the Sichuan Basin (China) due to biomass burning, whilst Lin *et al.* (2013)
101 reported an increase from 200 ppb to 600 ppb at Mei-Feng (Taiwan) due to the outflow
102 of smoke from South East Asia. Besides affecting air quality and increasing the risk of
103 death from respiratory causes (Jerrett *et al.*, 2009), O_3 is a short-lived climate forcer
104 (residence time of the order of several weeks in the free-troposphere, Monks *et al.*, 2015).
105 Hence, mitigating O_3 levels has two-fold benefits: reducing the impacts on air quality and
106 climate.

107 Atmospheric emission data for Brazil are rare and reliable emission inventories remain
108 elusive. However, the NOx and non-methane hydrocarbons (NMHC) estimates from
109 biomass burning and the road transport sectors provided by the EDGAR v4.2 database
110 (Crippa *et al.*, 2018) reveal the importance of biomass burning for atmospheric chemistry.
111 The NOx emissions from savanna, agricultural waste, forest and grassland fires in 2008
112 were 434.14 Gg whilst the road transport sector emitted 1,270 Gg. In terms of NMHC,
113 the figures are 839.4 and 1,250 Gg, respectively. However, considering that the fires in
114 Brazil occur mainly over three months, the emissions from the road transport should be
115 scaled accordingly to make a fair comparison. If we divide the annual road transport NOx
116 and NMHC emissions by four, we obtain 317.5 and 312.5 Gg, respectively, over three
117 months, which suggests that emissions from biomass burning make up a substantial
118 fraction of the precursors for O_3 formation.
119 In this study, we present a four-year climatology of O_3 for the states of São Paulo and
120 Paraná (Brazil), using ground-based *in situ* observations. We quantify the contribution of
121 long-range transport on the O_3 concentration in cities of different sizes by analysing the

coupling between O_3, NO and NO_2. We assess the impact of long-range transported smoke from central Brazil on the air quality by investigating a pollution outbreak within the most polluted months of 2015. We analysed the *in situ* data in combination with co-pollutants (NOx, $PM_{2.5}$ and PM_{10}), satellite retrieved aerosol optical depth, fire spots and airmass backward trajectories.

2. Methodology and data analysis

2.1 Study area

São Paulo is one of the 27 Brazilian federal units, located in the South Eastern region. It is the wealthiest and most populous state, accounting for 33.9% of the country's total GDP (Gandhi *et al.*, 2017) and hosting approximately one fifth of the country's population (45 million inhabitants). The state of São Paulo's economy is diversified and the chemical, sugar and ethanol production, metalworking, machinery, automobile and aviation industries account for 75% of the economic sector (Governo do Estado de São Paulo, 2019). The state has the largest vehicular fleet in the country, with 28.6 million units (DENATRAN, 2018) that emitted 331, 180, 5 and 4.7 Gg of CO, NO_x, PM and SO_2, respectively, in 2016. About 60% of these emissions occurred in the municipalities that form the metropolitan area of São Paulo (MASP), the cities of Campinas, Sorocaba, and urban agglomerations in Baixada Santista and Vale do Paraíba (CETESB, 2017). The vehicular emissions of NOx and total hydrocarbons (THC) dominate at state level (65 and 87%, respectively) and in the MASP (75 and 87%, respectively), which emphasises the effect this sector may have on local air quality.

2.2 Data

We used a combination of ground-based *in-situ*, remote sensing and modelling data to investigate the O_3 climatology at sites in the states of São Paulo and Paraná from 2014 to 2017. The *in situ* data are from 25 sites managed by São Paulo State Environmental Company (CETESB) and from Londrina, a mid-sized city located in the neighbouring state of Paraná (Fig. 2). The CETESB monitors criteria air pollutant with methods that follow closely those of the US Environmental Protection Agency. The data from Londrina were collected at the campus of the Federal University of Technology (UTFPR). A full list of the cities included in this study is provided in Table S1 (Supplementary Material). Note that Brazilian air quality networks are not designed for remote or rural conditions, like the sites in Europe (*e.g.*, Targino *et al.*, 2013; Witham and Manning, 2007). Instead, they are located in the urban core, close to highly-trafficked streets or industrial areas. This means that the analysis of long-range transport of air pollutants is more challenging, since the regional contribution cannot be easily isolated from local urban contributions.

The MODerate resolution Imaging Spectroradiometer (MODIS) Aqua and Terra Collection 6.1 Level 2 standard 10-km products were used here for best quality retrievals (quality flag = 3) of aerosol optical depth (AOD) over land. The data were obtained through NASA Goddard Space Flight Center's Atmosphere Archive and Distribution System (http://ladsweb.nascom.nasa.gov). Detailed descriptions of the MODIS dark target algorithm for retrievals of AOD over land can be found in Levy *et al.* (2013; 2007). Fire spots were identified by satellite remote sensing furnished by the National Space Research Institute of Brazil (http://www.inpe.br/queimadas/bdqueimadas) (INPE, 2018). Infrared radiation at 3.7 and 4.1 μm emitted from the fires is detected by the Advanced very-high-resolution radiometer (AVHRR) on board the polar-orbit satellites NOAA-15, NOAA-18, NOAA-19 and METOP-B, MODIS on board TERRA and AQUA, VIIRS on board NPP-Suomi and the geostationary satellites GOES-13 and MSG-3. The product

identifies spots at least 30 m long, occurring on non-cloudy days and with fire outbreaks lasting long enough to be captured between images.

To assess influences of atmospheric large-scale circulation on the air quality at the sites, five-day backward trajectories that arrived at 500 m above terrain level were calculated with 1-hour interval, eight times per day (00, 03, 06, 09, 12, 15, 18, 21 h), using the Hybrid Single Particle Lagrangian Integrated Trajectory Model (HYSPLIT) (Stein *et al.*, 2015). ERA-Interim reanalysis data of diagnosed boundary layer height, with three-hour time resolution, was taken from the European Centre for Medium-Range Weather Forecasts (ECMWF). We use meteorological data (air temperature, relative humidity, solar irradiance, wind speed and direction and atmospheric pressure) measured at UTFPR campus and at CETESB sites.

2.3 Cluster analysis

We applied hierarchical cluster analysis to reduce the number of observations and to find groups of similar stations within the O_3 dataset. We used O_3 concentrations due to the large data availability and its relatively long residence time in the atmosphere, which makes it a good tracer of long-range transported pollution. This technique was successfully used by Lyapina *et al.* (2016) to classify surface O_3 data over 1,400 European monitoring stations.

The hourly O_3 concentration for 26 sites in the period 2014-2017 yielded a matrix of 34,560 rows and 26 columns. The hierarchical clustering procedure starts with each site in its own group, which is progressively merged with the most similar site until all sites are in a single group. Observations that are as homogeneous as possible are collected into a group (large intra-group similarity), whilst keeping between-group (inter-group) observations as heterogeneous as possible (Hair *et al.*, 1998).

We used Ward's minimum variance method as merging criterion, since it has been widely used for climatic classifications with superior performance compared to other methods (*e.g*, Kalkstein and Corrigan, 1986). Ward's method starts with *K* groups (in our case, *K* sites) and at each step it fuses groups based on an error function that leads to a minimal within-group sum of squared distances (*W*) between the points and the centroids of the merged groups (Wilks, 2011). This means that the pair to be merged must minimise the sum of the squared distances between the data points and the centroids of their respective groups, summed over the resulting groups (Wilks, 2011):

$$W = \sum_{k=1}^{K} \sum_{j=1}^{J} \sum_{i=1}^{N} \left(x_{ijk} - \bar{x}_{jk}\right)^2, \qquad 1$$

where x_{ijk} is the *i*-th O_3 concentration of the *j*-th site in the *k*-th group, *J* is the number of sites, *N* the number of observations, and $\bar{x}_{jk}$ is the mean O_3 concentration inside this group. Ward's method computes *W* and *W'* before and after the merging, respectively, and merges clusters with the smallest $\Delta W = W' - W$.

We applied two approaches to decide on the number of clusters: the elbow and silhouette methods. The elbow method consists in running the clustering algorithm for a range of number of clusters (*n*) and calculating *W* for each *n*. *W* decreases monotonically as the number of *n* increases, and the *W* vs. *n* plot usually shows a bend which can be taken as a cut-off point to determine the number of clusters. From that point on, the *W* decrease flattens, indicating small changes and exaggerated specificity in the choice of clusters by increasing *n* (Lyapina *et al.*, 2016). The silhouette method (Rousseeuw, 1987) provides a graphical representation and an index to measure how well each object lies within its cluster. The silhouette value (*s*) lies between +1 (the object is correctly clustered) and -1 (the object belongs to other cluster).

2.4 Urban and regional contributions to the O_3 concentration

To estimate the regional contribution of O_3 to the *in situ* O_3 concentration, we calculated the daylight mean mixing ratios (in ppb) of the oxidant ($OX = O_3 + NO_2$) and NOx (Clapp and Jenkin, 2003). The analysis assumes that the interconversion of O_3, NO_2 and NO occurs in a closed system, where the total mixing ratio of both NOx and OX is unchanged. This photostationary state is valid during daylight, hence we considered the hours between 08:00 and 18:00.

Then, a linear regression analysis was performed between OX and NOx concentrations, where the offset can be interpreted as NOx-independent and the slope as NOx-dependent contributions. The former is attributed to regional background O_3 and the latter accounts for the local contribution, which correlates with the level of primary pollution. Any local change in NOx concentration will lead to a simultaneous increase or decrease in the concentration of total oxidants (Pancholi *et al*., 2018; Mazzeo *et al.*, 2005; Clapp and Jenkin, 2003). To investigate this aspect, we chose one city within each cluster with concurrent NOx, NO_2 and O_3 measurements.

3. Results

3.1 Overall O_3 concentrations in different time domains

Figure 1a depicts a statistical summary of O_3 concentrations at all sites between 2014 and 2017. The lowest O_3 concentrations were recorded in June and the highest in September and October. The air quality in South Eastern Brazil is affected by smoke plumes from the Amazon and Cerrado with peak activity in September, caused by the atmospheric transport under the influence of lingering high-pressure systems, which increases air temperatures and enhances photochemistry (Rosário *et al.*, 2013). Another source of air

pollution is the interhemispheric transport of plumes from Africa to Eastern South America, especially in September, October and November, enhancing the tropospheric O_3 column up to 40 Dobson Units (Ziemke *et al.*, 2011).

The stratosphere-troposphere intrusion is a well-documented phenomenon since the early 1960s (Junge, 1962). However, this mechanism is not common in the Southern hemisphere, with the exception for some hotspots observed in June, July and August over the East and West coasts of Australia, and from September to February over the Andes and the southern tip of Africa (Škerlak *et al.*, 2014). Figure 1b suggests a small variation in O_3 amongst the years investigated. However, the Krustal-Wallis test applied at the 5% significance level showed that there are statistically significant differences in O_3 between the years. These differences may be caused by fumigation of upper air masses that is influencing the boundary layer and surface O_3 concentrations, the number of fire outbreaks, regional transport and photochemistry. These mechanisms will not be addressed in this manuscript. The O_3 concentration was consistently higher in the spring months (September and October) for all years investigated in the present study (Fig. 1c).

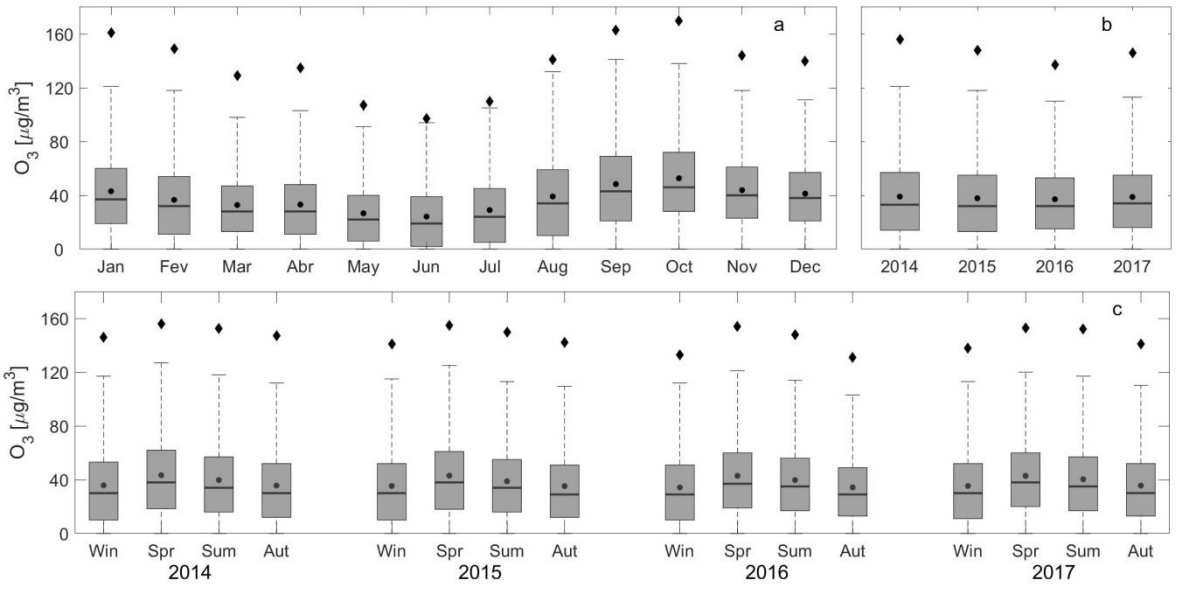

Figure 1: Statistical summary of hourly O_3 concentration from 2014 to 2017 for all sites, with respect to a) month, b) year and c) season disaggregated per year. The dots indicate

the mean values, the diamonds are the 99.5 percentile, the whiskers are the 5th and 95th percentiles, the box limits are the 25th and 75th percentiles and the black lines across the boxes are median values.

3.2 O_3 data reduction based on cluster analysis

The elbow method suggested that the O_3 dataset measured at the 26 sites could be divided into either five or six clusters. However, the silhouette method revealed that choosing six clusters would yield negative *s* values and an overall decrease in the *s* values (between 0.1336 and 0.4660 for five clusters, and between 0 and 0.4324 for six clusters). Another aspect that we also considered to maintain five clusters was the consistency in the location of the stations within each regional area. Figure 2 shows that the stations are distributed across three main areas **Inland:** clusters 1, 2 and 5 (C1, C2 and C5), **Coast:** C3, and **Greater São Paulo and East:** C4.

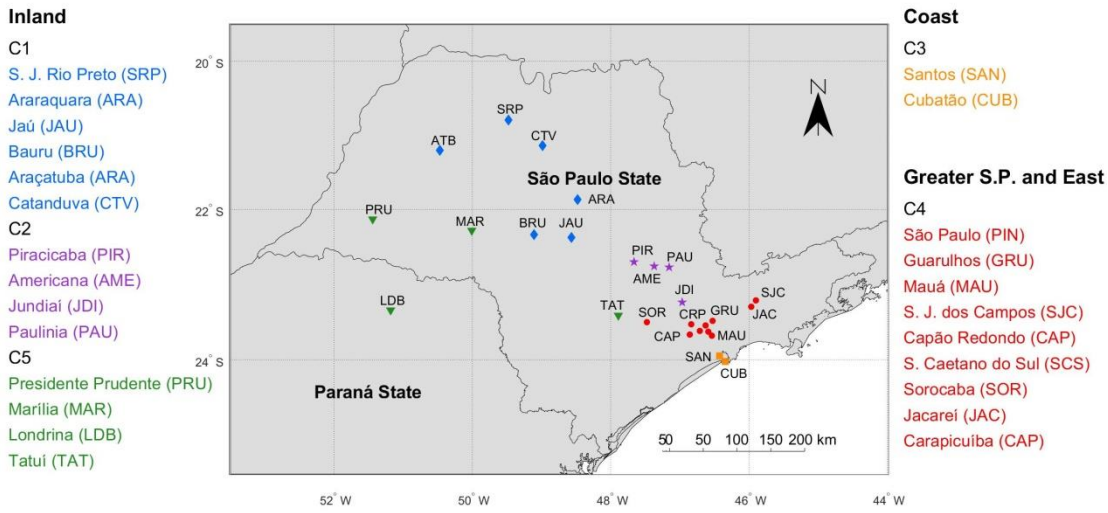

Figure 2: Location of the sites investigated in this study. The colours indicate the groups as determined by the cluster analysis and the symbols diamond, star, square, circle and triangle correspond to the groups C1, C2, C3, C4 and C5, respectively.

Figure 3a shows statistic summaries of O_3 for the individual clusters using the datasets from 2014 to 2017, organised in descending order of median values. Overall, the largest O_3 concentrations were recorded at the inland sites and the lowest concentrations at the coastal sites, with mean values varying from 25.2 to 47.6 μg/m^3 and medians from 18.0 to 43.0 μg/m^3. Even though C2 on average was not the most polluted cluster, the stations in this group had the largest interquartile range and 95th percentile. This suggests that the sites within this group were affected by events causing frequently extreme O_3 concentrations. The mean daily O_3 concentrations per cluster (Fig. 3b) showed similar patterns with a large interannual variability along the years investigated. The intercluster correlations using monthly mean O_3 concentrations were statistically significant (*p* values much smaller than 0.05) with Pearson's correlation coefficients (r) between 0.75 (C3 and C5) and 0.93 (C2 and C4).

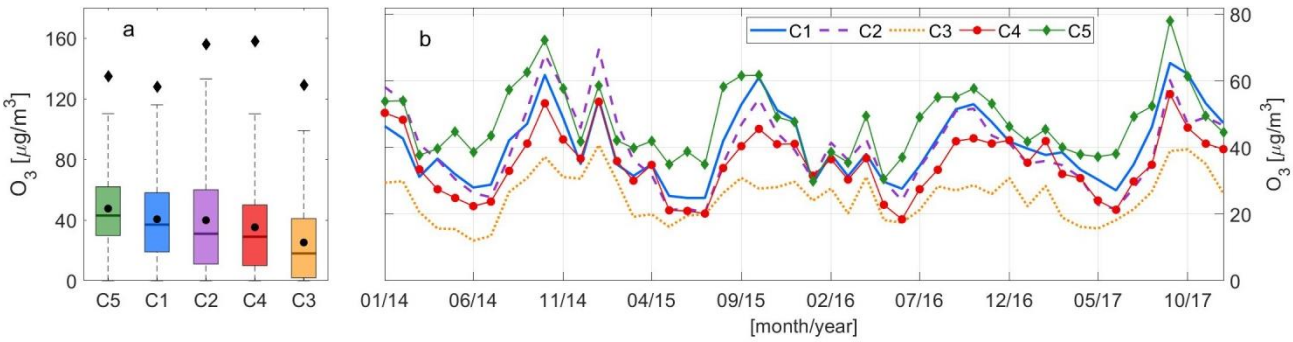

Figure 3: (a) Statistical summary of O_3 data for the clustered stations. The dots indicate the mean values, the diamonds are the 99.5 percentile, the whiskers are the 5th and 9th percentiles and the box limits are the 25th and 75th percentiles and the black lines across the boxes are median values. (b) Mean monthly O_3 concentrations segregated per cluster in the period 2014 – 2017.

3.3 Seasonal, weekly and diurnal profiles of O_3 concentrations

Figure 4a shows that the monthly mean O_3 concentration vary seasonally for all clusters, with an increase that begins in July and peaks in September or October. C5 is by far the most polluted cluster from April to September. The comparison between C5 and C3 is particularly striking, with differences in O_3 concentrations of 13.0 and 31.3 $\mu g/m^3$ in January and September, respectively. Another outstanding feature is that whilst the O_3 concentrations for C1, C2, C3 and C4 show a clear decrease between January and June, the concentration for C5 remain relatively stable and fluctuate between 36.2 and 43.2 $\mu g/m^3$. Comparatively, the concentration for C4 more than halved over the same period (from 43.1 to 20.8 $\mu g/m^3$).

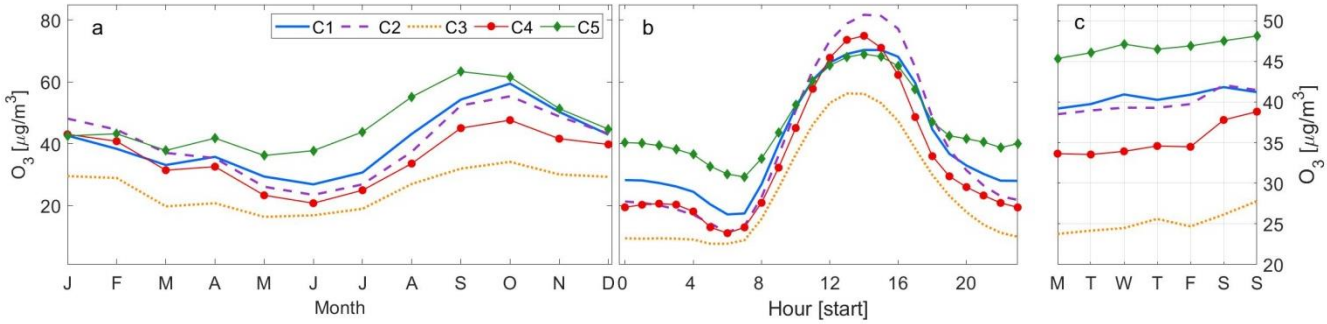

Figure 4: (a) Monthly, (b) diurnal and (c) weekly mean O_3 concentrations for the clustered stations.

The clusters show rather similar diurnal patterns, with peak O_3 values in the early afternoon (13:00-15:00, Fig. 4b), with C2 and C4 having the largest peaks and C3 the lowest. C2 and C4 consist mostly of mid-sized and large cities, with traffic volumes that emit large amounts of NOx. However, the reduction of NO emissions relative to NO_2, typical in urban environments, decreases the NO titration effect and increases the daytime O_3 concentration (Querol *et al.*, 2016). This effect was more pronounced for C4, which contains larger cities (including those that form the MASP) and larger vehicle fleets

(Table S1, Supplementary Material). At night, O_3 decreases due to the cease of production, loss mechanisms (dry deposition on the ground) and titration by NO (Monks *et al*., 2015). C1 and C5 have comparable daytime mean O_3 peak concentration of about 70 $\mu g/m^3$, but diverge at night with concentrations for C5 up to 12 $\mu g/m^3$ greater than for C1. C5 has an outstanding secondary nocturnal O_3 peak and the smallest diurnal range. Krecl *et al.* (2016) also observed a secondary O_3 maximum at night in Londrina (a site within C5), which they attributed to horizontal and vertical transport of O_3 from other regions.

The inspection of the diurnal cycle with respect to month showed that this feature prevails along the year and intensifies in September with a maximum nocturnal peak of 55 $\mu g/m^3$ (Fig. S1, Supplementary Material). Comparatively, the mean maximum diurnal peak was 92 $\mu g/m^3$ at 15:00 in the same month. We hypothesise that two phenomena may control this feature within this group: (i) C5 consists mostly of small cities, Marília (pop. 237,000), Presidente Prudente (pop. 208,000) and (Tatuí, pop. 120,000) (except Londrina, pop. 564,000), that have relatively small traffic volumes to furnish NO and to effectively destroy O_3 at night. Although Londrina's fleet amounts to about 387,000, the sampling site was on the city's outskirts, with little influence from direct vehicular emissions. (ii) Persistent transport of aged pollutants from other regions contributes to a rise in the O_3 nocturnal base line during the year, which is intensified in the spring months due to pollution outbreaks. One pathway is the advection of O_3 from large urban conglomerations, such as MASP. Boian and Andrade (2012) conducted a study using a photochemical model and pinpointed that a nocturnal O_3 peak of 176 $\mu g/m^3$ (at 22:00 h) in Campinas (northwest of the city of São Paulo) was due to a plume from the MASP, which still lingered in the early hours. The cities in cluster C5 are all located west of the MASP, and according to INMET (2018) the prevailing wind directions in Presidente

Prudente and Londrina (both within C5) are easterly and easterly/southeasterly, respectively. More precisely, Krecl *et al.* (2016) observed easterly components in Londrina between 00:00 and 10:00 h.

C3 is the cleanest cluster and although Santos and Cubatão have a relatively large fleet (a combined total of 331,600 vehicles) and Cubatão is an industrial city with a cluster of petrochemical, steel and fertilizer industries, they are located on the coast, where frequent overcast weather reduces the incoming solar radiation and inhibits photochemical processes. The mean annual insolation for Santos is 1,376 h with 70% of cloud coverage. For comparison, Londrina in C5 has mean annual insolation of 2,420 h and 50% of cloud coverage (INMET, 2018).

Figure 4c shows that the O_3 concentration tend to increase at weekends, following what has been coined "the ozone weekend effect" (Heuss *et al.*, 2003), attributed to changes in precursors due to the decrease in the traffic volume and travelled distances. Vukovich (2000) and Altshuler *et al.* (1995) showed that the reduction in NOx at weekends is more pronounced than for VOC, favouring the O_3 formation due to an increase in the VOC:NOx ratio The weekend effect was more evident for clusters C3 and C4 (Table 1) that consist of highly urbanised areas and have large vehicle fleets. We did not have VOC measurements in this study; however, we refer to the results by Orlando *et al.* (2010) who measured VOC in the MASP and reported a high VOC:NOx ratio, especially due to formaldehyde and acetaldehyde. They used model simulations to show that an increase (decrease) in VOCs would result in an increase (decrease) in O_3. Hence, we suggest that this effect combined with the reduction in O_3 loss due to less titration with NO (Atkinson-Palombo *et al*., 2006; Torres–Jardon and Keener, 2006; Alghamdi *et al*., 2014) yields higher O_3 concentrations at weekends within these clusters.

374 Other pathways for the O_3 weekend effect include: (i) the shift in the timing of NOx peak
375 favours O_3 formation at weekends than on weekdays), (ii) carryover of pollutants with
376 higher VOC:NOx ratios from light-duty vehicle traffic on Friday and Saturday evenings
377 that can generate more O_3 at weekends, (iii) lower aerosol concentrations at weekends
378 increase incoming solar radiation and photochemistry (Heuss *et al.* (2003).
379
380 Table 1: O_3 concentrations in different time domains, derived from hourly mean data.

O_3 [$\mu g/m^3$]	C1	C2	C3	C4	C5
Diurnal range[a]	53.1	70.3	48.6	63.8	39.7
Diurnal maximum[b]	70.3	81.7	56.3	74.9	69.0
Seasonal range (October - January)[c]	32.6	31.9	17.8	26.8	23.8
Sunday-Monday difference[d]	2.0	3.0	4.0	5.2	2.8

381 [a]Based on the difference between the mean maximum and minimum diurnal O_3 concentrations.
382 [b]Maximum O_3 concentration of the diurnal cycle. [c]Based on the difference between the mean
383 monthly O_3 concentrations in October and January. [d]Based on the difference between the mean
384 concentrations for all Sundays and all Mondays.
385
386 **3.4 Pollution outbreak in September 2015**
387 In the austral spring of 2015 an area of about 225,300 km^2 was burned in Brazil, of which
388 56.0% and 24.5% comprised Cerrado and Amazon biomes, respectively (INPE, 2018).
389 Figure 5 shows MODIS AOD scenes for September 23rd 2015 over South America (left)
390 and daily AOD time series along this year (right). It is clearly discernible that enhanced
391 levels of aerosols began to influence the central part of Brazil (right, upper panel) and the
392 state of São Paulo (right, lower panel) in August until the end of the year.

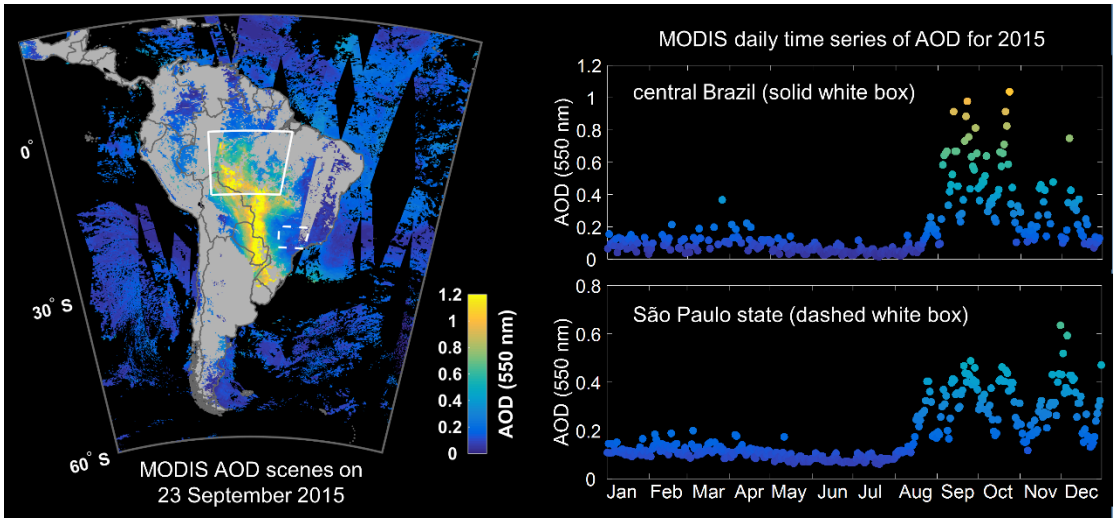

Fig. 5: MODIS Aqua and Terra AOD scenes over South America for September 23rd 2015 (left), and daily time series of AOD for the central Brazil and the state of São Paulo (right).

We focus here on an air pollution outbreak that led to an enhancement in O_3 concentration and other co-pollutants over the investigated area during the second half of September 2015. Figure 6a shows that the O_3 concentration started to increase around September 15th for all clusters, with enhancements between two- and four-fold: for example, from 48.0 to 103.5 μg/m^3 within C3 and from 38.0 to 169.8 μg/m^3 within C4, between September 11th and 20th. Meteorological data measured at UTFPR campus in Londrina (C5) show that the substantially higher O_3 concentrations that occurred in the afternoon during the period September 14th-25th coincide with a high-pressure system that led to high temperatures, low relative humidity and strong solar irradiance (for example, > 35 ºC, < 20% and > 1,000 W/m², respectively, in the afternoon of September 23rd) (Figures 6b-6d). Such a meteorological situation causes subsiding air to warm adiabatically, inhibits convective mixing and creates a shallow boundary layer where pollutants can accumulate. This is in line with Pudassainee *et al.* (2006) who showed that O_3 production is favoured by increase in air temperature and solar irradiance, and with Querol *et al.*

411 (2016) who reported very high O_3 concentrations during heat waves in Spain in the
412 summer of 2015.
413 The surface winds measured at UTFPR campus between September 16^{th}-19^{th} were
414 northerly and larger than 5.0 m/s in the afternoon, which facilitated advection of polluted
415 air. Between September 20^{th}-23^{rd} the mean wind speed dropped to 2.7 m/s (Fig. S2,
416 Supplementary Material), reducing the air pollution dispersion and facilitating their
417 accumulation.
418 Although Figs. 6b-6d illustrate the weather conditions in Londrina, the corresponding
419 meteorological variables correlate well with data from sites within other clusters (see
420 Figs. S3-S8, Supplementary Material). For example, the Pearson's correlation coefficient
421 for hourly air temperature between Londrina and São José do Rio Preto (distance 390 km)
422 and between Londrina and the city of São Paulo (distance 540 km) during the pollution
423 outbreak were 0.95 and 0.91, with linear regression equations of 1.1x-0.29 and 1.0x-2.9,
424 respectively, and *p*-values much smaller than 0.05. Only Santos (distance 600 km from
425 Londrina) showed a more modest air temperature increase, yielding weak or moderate
426 correlations with other sites, possibly due to local atmospheric circulations embedded in
427 the large-scale circulation (for example, sea breeze).
428

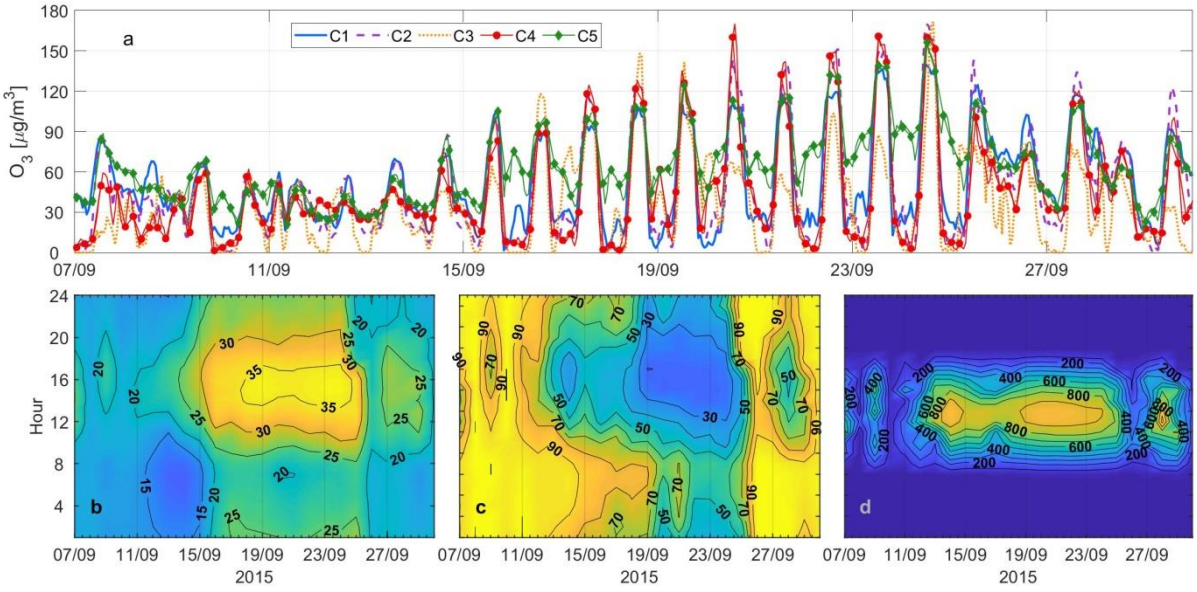

Fig. 6: (a) Hourly mean O_3 concentration segregated per cluster, (b) air temperature, (c) relative humidity and (d) solar irradiance measured in Londrina (C5) for the case study in September 2015.

Figure 7 suggests that air masses that arrived at 500 m above ground level in Londrina in the period September 9th-13th (prior to the pollution event) had either maritime origin or mainly passed over land areas unaffected by fire spots (red dots).

Areas closer to the receptor point were highly influenced by fires from September 15th (Fig. 7). Four days prior to and during the pollution events (September 7th-14th and September 15th-24th, respectively), the mean AOD and corresponding one standard deviation for the state of São Paulo (20-24ºS, 45-52ºW) were 0.23±0.07 and 0.39±0.06, respectively. Satellite data provided by INPE indicated an increase of 42% in the occurrence of fire spots in Brazil in the episode period compared to the non-episode period. Particularly, the numbers of fire spots in the states of Paraná and São Paulo increased from 316 to 2,719 and from 68 to 2,302 spots, respectively (Figs. S9 and S10). Table 2 displays statistics of O_3 concentration within each clusters before and during the pollution event.

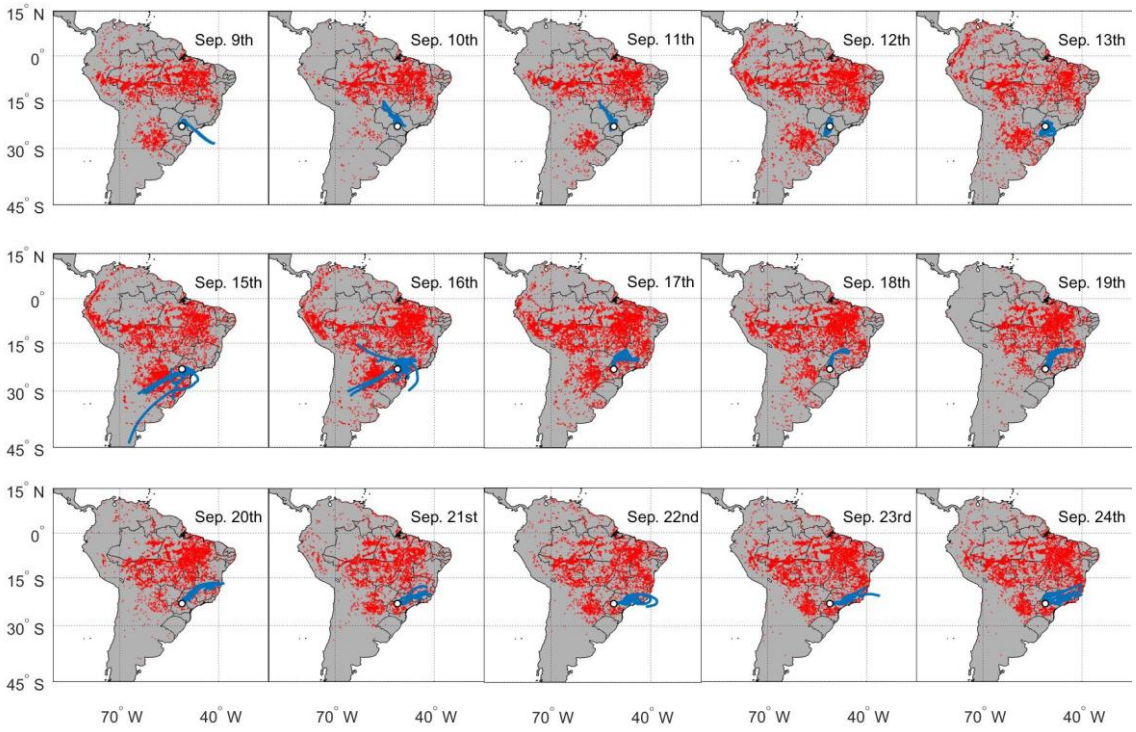

447

448 **Fig. 7:** Fire spots (red dots) over South America and five-day backward trajectories (blue
449 solid lines) before (first row) and during the pollution outbreak (second and third rows).

450 Table 2: Comparison of mean hourly (± one standard deviation) and maximum O_3
451 concentrations before and during the pollution outbreak in September 2015.

452

O_3 [$\mu g/m^3$]	C1	C2	C3	C4	C5
	Before the pollution outbreak				
Mean	40.4 ± 17.0	34.1 ± 20.6	24.4 ±17.6	30.0 ± 15.1	43.9 ± 14.4
Maximum	85.8	87.2	58.0	74.0	88.6
	During the pollution outbreak				
Mean	54.4 ± 40.4	54.2 ± 49.0	43.4 ± 38.2	52.4 ± 49.0	79.8 ± 28.5
Maximum	140.3	169.8	171.5	170.0	156.2

453

The pollution outbreak was captured across the state of São Paulo, as shown by the evolution of O_3, NOx, $PM_{2.5}$ and PM_{10} at sites representative of each cluster (Fig. 8 and Table 3): São José do Rio Preto (C1), Piracicaba (C2), Santos (C3), São Paulo (C4) and Marília (C5). During this event, a large increase in nocturnal O_3 concentration was observed in Marília and Santos. The results on diurnal cycles (Section 3.3) had already revealed that C5 presented a secondary nocturnal O_3 peak. However, the peak recorded in Marília during this pollution outbreak (> 100 μg m^{-3} on September 23rd) was much larger than observed even in the dirtiest month (Fig. S1, Supplementary Material). The nocturnal peak observed in Santos (> 60 μg m^{-3}) was an uncommon feature compared to the diurnal cycle for C4. The enhancement of NOx was observed at all sites, especially at night, due to the increase in NO_2 via NO-to-O_3 conversion, with mean episode:non-episode NOx ratios ranging from 1.4 (Santos) to 3.5 (São José do Rio Preto). The particulate concentrations showed a very sharp increase starting on September 15th, with higher concentrations occurring generally in the early morning and late evening hours. The diurnal variation was due to the increase in the boundary layer height in the afternoon –which favours dilution of the pollutants– and by a shallow layer in the evening, as shown by three-hour resolution ERA-Interim reanalysis data taken from the ECMWF (Fig. S11). Pollutant concentrations greatly exceeded the thresholds recommended by the World Health Organisation (WHO), whereas in a few occasions were the Brazilian air quality standards for $PM_{2.5}$ and PM_{10} (60 and 120 μg/m^3, respectively) exceeded. This occurred only once at Pinheiros in Greater São Paulo and Piracicaba on September 24th (65.5 and 134.2 μg/m^3, and 62 and 141 μg/m^3, respectively). However, all clusters exceeded the daily WHO limits for $PM_{2.5}$ or PM_{10} (25 and 50 μg/m^3, respectively) at least five out of 10 days of the duration of the event (São José do Rio Preto exceeded the PM_{10} limit on 10 days). Santos, on the other hand, surpassed the PM_{10} limit only once (53 μg/m^3 on

September 24th). McClure and Jaffe (2018b) found that wildfires caused a significant increase in the 98th quartile $PM_{2.5}$ concentrations at sites in the northwest United States (average 0.21 ± 0.12 μg/m^3/year), and Targino *et al.* (2013) reported that the concentration of accumulation-mode particles increased by 40 and 340% at urban and rural sites, respectively, in Sweden due to the outflow of wildfire plumes from Eastern Europe.

The Brazilian standard for O_3 (maximum daily 8-hour moving mean of 140 μg/m^3) was exceeded only in Marília (three days), Piracicaba (four days) and São Paulo (one day). However, when considering the WHO guideline of 100 μg/m^3, Marília exceeded the limits on all days investigated here, Piracicaba on eight days, São Paulo on four days and São José do Rio Preto on three days. As the increase in O_3 was accompanied by substantial increase in both $PM_{2.5}$ and PM_{10}, it is evident that the long-rang transport of smoke severely deteriorates the air quality in cities of all sizes, and can outweigh measures to curb local air pollution.

Cluster	Site	O_3			NOx			$PM_{2.5}$			PM_{10}		
		($\mu g/m^3$)											
		Mean	P5	P95	Mean	P5	P95	Mean	P5	P95	Mean	P5	P95
C1	**São J. Rio Preto**												
	Non-episode	41.2	11.1	79.9	11.1	3.0	27.9	12.3	1.1	30.0	22.9	6.1	58.8
	Pollution outbreak	[a]41.5	[a]1.0	[a] 118.9	38.9	4.0	125.0	27.0	9.0	50.5	65.8	29.5	118.5
C2	**Piracicaba**												
	Non-episode	41.7	4.1	89.0	n.m.	n.m.	n.m.	11.8	3.0	25.0	24.8	9.0	57.8
	Pollution outbreak	61.1	3.0	157.5				25.3	10.0	43.0	78.2	30.0	138.5
C3	**Santos**												
	Non-episode	24.3	1.0	54.8	24.4	4.0	64.9	11.4	1.0	27.0	15.8	3.0	36.0
	Pollution outbreak	39.0	1.0	91.0	34.7	4.0	110.0	25.3	4.0	51.8	36.4	10.0	74.0
C4	**S. Paulo (Pinheiros)**												
	Non-episode	23.3	0.9	50.0	41.2	12.6	86.9	11.1	1.0	26.2	16.4	1.0	44.6
	Pollution outbreak	39.7	1.0	131.0	103.2	12.1	284.6	25.3	1.5	66.2	49.0	9.0	84.1
C5	**Marília**												
	Non-episode	52.7	23.0	83.0	7.2	2.0	17.0	n.m.	n.m.	n.m.	14.7	4.0	37.1
	Pollution outbreak	96.8	41.0	150.0	12.4	3.0	37.5				36.6	19.0	53.0

493 Table 3: Summary of pollutant concentrations during the non-episode (September 7th-14th) and pollution outbreak (and September 15th-24th) periods

494 for sites representative of each cluster.

495

496 [a]This value may not be representative due to reduced number of observations. n.m. Not measured at this site.

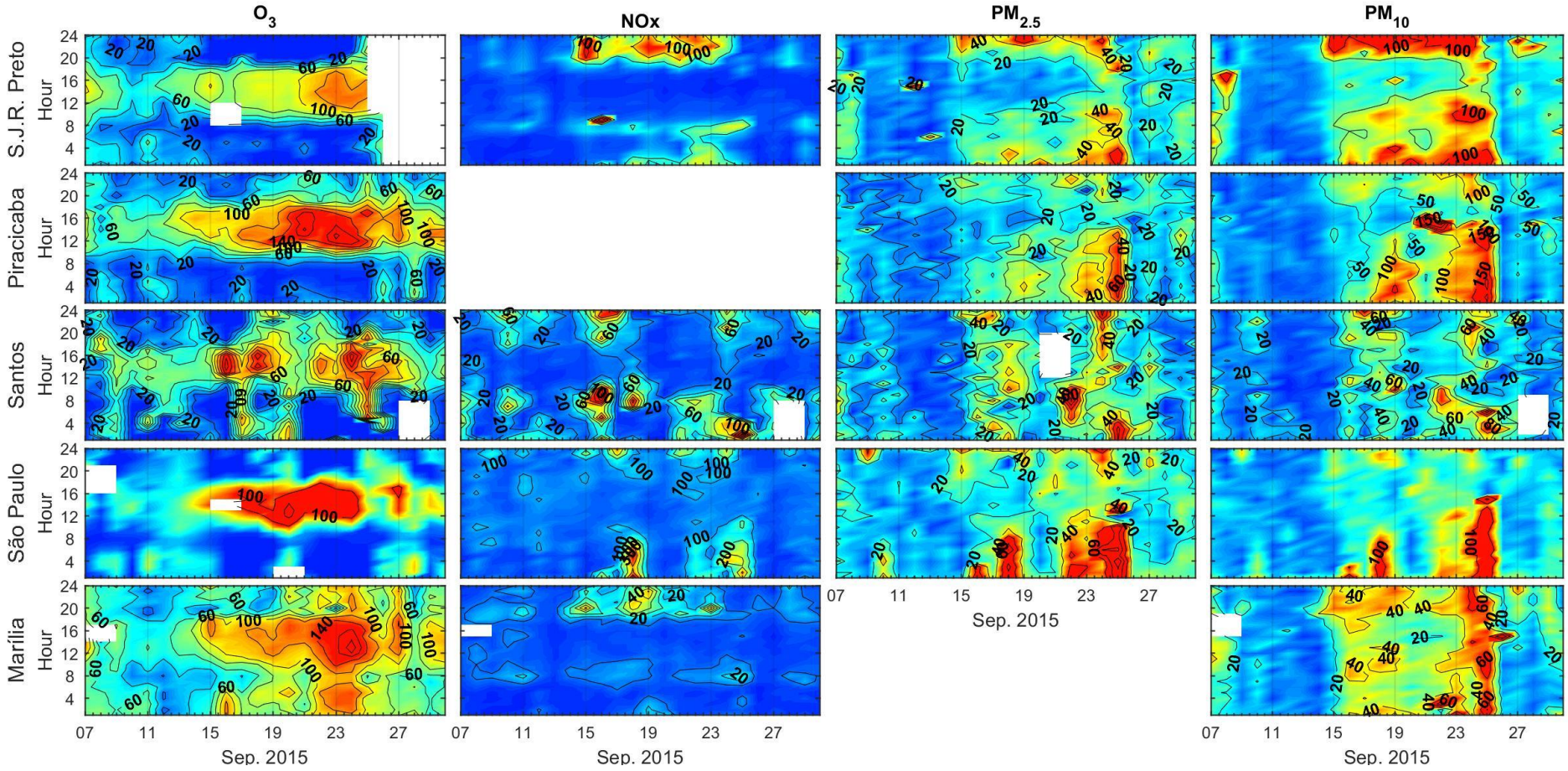

Fig. 8: Hourly O_3, NOx, $PM_{2.5}$ and PM_{10} concentrations measured in September 2015 at selected sites in the state of São Paulo.

3.5 OX analysis and estimates of local and long-range contribution

To disentangle the local and regional contributions of O_3 across the study area, we picked the cities discussed in the previous section due to the availability in NOx, NO_2 and O_3 measurements. Besides analysing the NOx-OX relationship for all sites and months we split the data into three-month periods, since we observed that August, September and October were the most polluted months (Fig. 4a). We grouped the months as follows: (i) February, March and April, (ii) May, June and July, (iii) August, September and October, and (iv) November, December and January.

Figure 9a shows the NOx-OX relationship for all sites irrespective of the time of the year, and Figs 9b-f subdivided with respect to site and season. Also shown are the linear regression equations and Pearson's correlation coefficient (for all cases, the *p*-values were much smaller than 0.05). We found a positive linear increase of OX with NOx, with a mean intercept of 31 ppb (60.8 $\mu g/m^3$), which can be interpreted as the regional O_3 contribution. This is in line with previous studies by Pancholi *et al*. (2018), Mazzeo *et al.* (2005) and Clapp and Jenkin (2003) who reported regional contributions of 59, 43 and 70 $\mu g/m^3$ for Jodhpur (India), Buenos Aires (Argentina) and London (UK), respectively. However, when inspecting our results with respect to site and season we found different strengths of the regional contribution (Figs. 9b-f). The largest regional O_3 contribution at all sites was found for the biomass burning season (August-October). Clapp and Jenkin (2001) also found that the regional contribution increased from 76 $\mu g/m^3$ on non-episode days to 109 $\mu g/m^3$ on episode days in London (the latter was defined as days in April-September affected by regional-scale photochemical events). We found that during the polluted season in South Eastern Brazil, small cities received a relatively large regional contribution. For example, the mean annual O_3 concentration (± one standard deviation) in Marília was only 26.1±12.6 ppb (51.2±24.6 $\mu g/m^3$). However, the regional transport

may account for as much as 41.4% of the total O_3 in Marília when considering the maximum concentration observed during the biomass burning season (99 ppb). The regional contribution of O_3 for Piracicaba, Santos, São Paulo and São José do Rio Preto, considering the most extreme O_3 concentrations in the same period (117.4, 65.8, 151.5 and 98 ppb, respectively) were 36.6, 38.0, 23.1 and 37.8%.

We found a large variability in local OX with respect to season, and the largest contribution was observed in summer at all sites (November-January). This term is contributed by primary NO_2 emissions, typically 5-15% of NO_x, and local O_3 formation, which depends on the sources of NOx. In urban areas, on-road transport are the dominating sources and NO_2 enters the atmosphere mostly via the reaction:

$$NO + O_3 \rightarrow NO_2 + O_2. \qquad \text{R1}$$

Hence, in most cases the local production will depend on the fleet characteristics, fuel composition and traffic volumes (Carslaw, 2005). However, a source apportionment study for the mega city of São Paulo showed a slightly different scenario in which not only exhaust from on-road transport, but also industrial activities and biomass burning (both local and remote) contributed to the air pollution in the city (Pereira *et al.*, 2017), and, thus, can be sources of NOx.

We found a large variability in local OX with respect to season, and the largest contribution was observed in summer at all sites (November-January). The smallest slopes were observed in São Paulo and Santos (< 1), regardless of the period of the year (see equations in Fig. 9 and S12 for a month-by-month variability). Clapp and Jenkin (2003) and Notario *et al.* (2012) showed that the local contribution at sites in the UK and

548 Spain also peaked in summer, which has been attributed to higher solar irradiance and
549 enhanced photochemistry.
550 We calculated the NO_2:OX ratios from hourly data and a positive trend was identified
551 with increasing NOx concentration (Fig. S13 Supplementary Material). According to the
552 mean NO_2:OX ratios, the selected sites can be classified within two groups: one with
553 mean ratios higher than 0.35 (São Paulo and Santos) and the second group with ratios
554 substantially lower (São José do Rio Preto, Marília and Piracicaba) (Table 4).
555

Cluster	Site	Feb-Mar-Apr	May-Jun-Jul	Aug-Sep-Oct	Nov-Dec-Jan
C2	**Piracicaba**	0.17±0.09	0.31±0.17	0.18±0.08	0.12±0.06
C4	**São Paulo**	0.49±0.19	0.67±0.18	0.51±0.17	0.40±0.17
C1	**São José Rio Preto**	0.20±0.08	0.28±0.12	0.21±0.13	0.21±0.19
C3	**Santos**	0.41±0.15	0.51±0.22	0.36±0.14	0.35±0.14
C5	**Marília**	0.16±0.06	0.23±0.09	0.14±0.06	0.14±0.08

556
557 Table 4: Summary of mean (± standard deviation) NO_2:OX ratios segregated by site and
558 season in the period 2014-2017.
559
560 The differences in the partitioning can be partially attributed to:
561 *(i)* Photochemical processes. The lower insolation in Santos and, to a lesser degree in São
562 Paulo (1,895 h/year) makes the reaction
563
564 $NO_2 + hv \rightarrow NO + O,$ R2
565
566 less efficient than at the other sites, since the rate of NO_2 photolysis is a function of solar
567 radiation intensity (actinic flux), which can be attenuated by cloud scattering. This effect

preserves NO_2 and increases the NO_2:OX ratio, especially in winter (May, June and July) (Table 4).

(ii) Proximity to exhaust emissions from diesel light-duty vehicles. Grange *et al.* (2017) showed a clear positive trend in NO_2 directly emitted by diesel passenger cars in Europe in the period 1995-2010, reaching about 15% of the total NOx in 2010. Although, current Brazilian regulations prohibit the sales of diesel passenger cars, light-duty vehicles for commercial purposes and sport utility vehicles (SUV) run on diesel and largely penetrated the Brazilian market since 2008. Nowadays, 46% of the sales of light-duty vehicles correspond to diesel-fuelled units and represent 6.8% of the total market sales (ANFAVEA, 2019). These vehicles have emission standards mostly equivalent to Euro 3, 4 and 5.

Despite the lack of studies on trends in the NO_2:NOx ratio for Brazil, we hypothesise that direct NO_2 emissions from diesel vehicles increased in recent years. This effect may have been captured by the measurements at São Paulo Pinheiros site, which is located on the kerb of Frederico Hermann street –a eight-lane road used for traffic and kerbside parking. Moreover, the site is only 230 m from the highly trafficked Marginal Pinheiros ring road, where congestion frequently occurs and the proportion of diesel-fuelled vehicles is high.

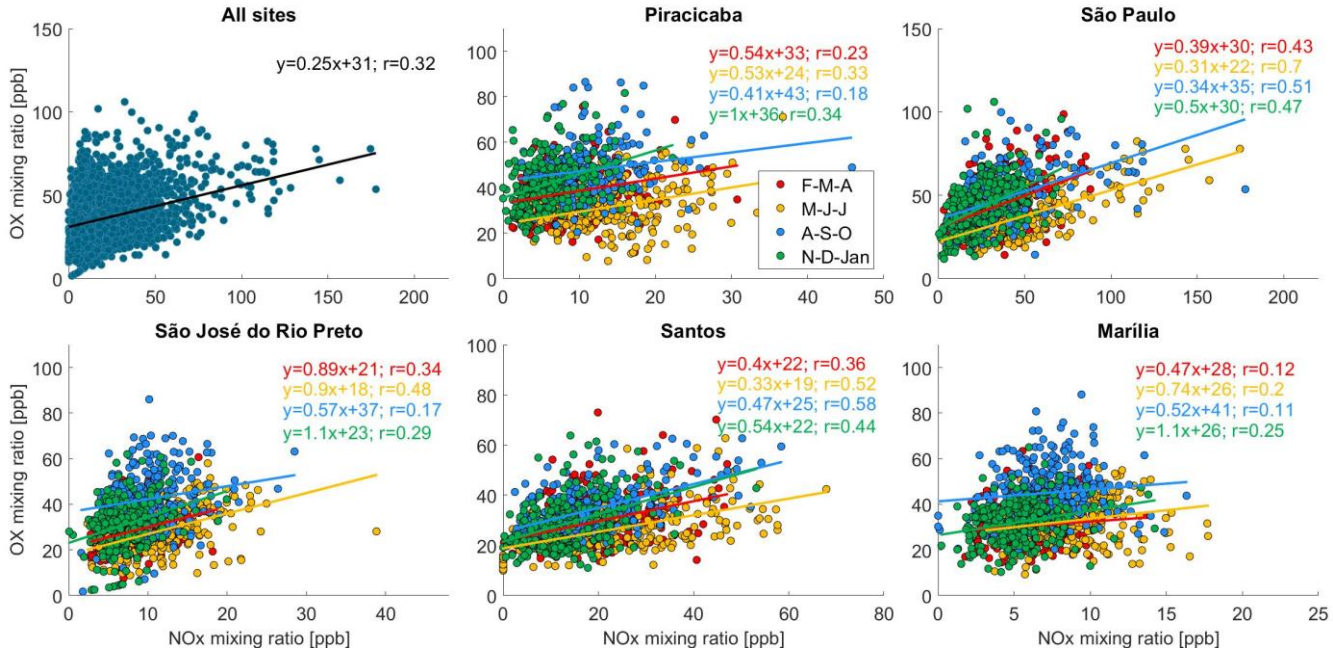

Fig. 9: Variation in mean daylight mixing ratios of OX with respect to NOx. The lines were obtained by linear regression analysis. Also shown are linear regression equations and the Pearson's correlation coefficient.

4. Summary and conclusions

Applying a hierarchical clustering technique on hourly O_3 data collected in the period 2014-2017 at 26 sites in the states of São Paulo and Paraná, Brazil, enabled us to reduce the dataset to five homogenous groups with respect to seasonal, monthly, weekly and diurnal concentrations. The cleanest group was located on the coast whilst the inland sites showed the highest concentrations. Group C5 (inland) stood out with a pronounced mean annual nocturnal O_3 peak of 40 $\mu g/m^3$, which reached 55 $\mu g/m^3$ in September. Comparatively, the mean annual diurnal peak was 63 $\mu g/m^3$. We attributed this peak to the combined effects of transported smoke from biomass burning and sustained outflow of aged pollution from the metropolitan area of São Paulo. All groups were associated with peak O_3 concentrations in September or October, with mean values between 34 and 63 $\mu g/m^3$, coinciding with the biomass burning season in central and northern Brazil. The

overall mean regional O_3 contribution during the polluted period was 61 $\mu g/m^3$, with a great seasonal and intersite variability, ranging from 35 to 84 $\mu g/m^3$. We found that the long-range transport of smoke can contribute with between 23 and 41 % of the total O_3. Investigation of a pollution outbreak in September 2015 showed that the smoke caused sharp increases in O_3, $PM_{2.5}$ and PM_{10} concentrations and exceedances in the levels recommended by the WHO. All cities were affected with between 2.2- and 3.1-fold increases in PM_{10}, 2-fold increase in $PM_{2.5}$, between 1.5- and 1.8-fold increases in O_3 and between 1.4- and 3.5-fold increases in NOx concentrations compared to the non-episode period. This indicates that biomass burning, both in remote and proximate areas, increases gas and particulate concentrations and quickly deteriorates the air quality of small and big cities. Depending on the large-scale circulation, the exceedances in air quality standards can last for several days and outweigh the reductions in anthropogenic sources that are promoted to curb air pollution in cities (for example, on-road traffic exhaust emissions). Analysis of the local oxidant sources showed a substantial variability across the study area and a seasonal dependence. More specifically, larger contributions in the period November-January due to enhanced photochemistry. The local oxidant contribution was lower in the cities of São Paulo and Santos, compared to the inland sites.

The state of São Paulo has always been at the forefront in terms of progressive measures to curb air pollution, by introducing programs to control sulphur dioxide from industrial sources and by enforcing standards for cleaner vehicles and fuels. However, the present results indicate that policies targeting the reduction of biomass burning is of outmost importance to improve the urban air quality, particularly in densely populated areas where high pollutant concentrations are frequently observed. This can only be achieved with enhanced governance acting at regional, national and international levels to combat biomass burning practices in Brazil and its neighbouring countries. Not only the

629 population health would benefit from such a measure, but also the regional climate, since
630 O_3, BC and $PM_{2.5}$ are short-lived climate forcers (SLCF).
631 This strategy would be well-aligned with the Paris Agreement that aims to limit global
632 warming to below 2 °C compared to pre-industrial, and which must be complemented
633 with the reduction of SLCF emissions.
634

635 **Acknowledgments**
636 The authors thank CETESB, ECMWF and INPE for providing data for this study and
637 Prof. Jorge Alberto Martins for furnishing the weather data collected at the campus of the
638 Federal University of Technology.
639

640 **Declaration of interest:** None
641

642 **References**

643 Akagi, S.K., Yokelson, R.J., Wiedinmyer, C., Alvarado, M.J., Reid, J.S., Karl, T.,
644 Crounse, J. D., and Wennberg, P.O., 2011. Emission factors for open and domestic
645 biomass burning for use in atmospheric models. *Atmos. Chem. Phys.*, 11, 4039–4072.

646 ANFAVEA, 2019. Brazilian automotive industry yearbook 2019

647 (http://www.anfavea.com.br/anuarios.html). Last accessed 24 April 2019.

648 Alghamdi, M.A., Khoder, M., Harrison, R.M., Hyvärinen, A.-P., Hussein, T., Al-Jeelani,
649 H., Abdelmaksoud, A.S., Goknil, M.H., Shabbaj, I.I., Almehmadi, F.M., Lihavainen,
650 H., Kulmala, M., and Hameri, K. 2014. Temporal variations of O_3 and NO_x in the
651 urban background atmosphere of the coastal city Jeddah, Saudi Arabia. *Atmos.*
652 *Environ.*, 94, 205-214.

Allen, A.G., Cardoso, A.A., Rocha, G.O., 2004. Influence of sugar cane burning on aerosol soluble ion composition in Southeastern Brazil. *Atmos. Environ.*, 38, 5025–5038.

Altshuler, S.L., Arcado, T.D., Lawson, D.R., 1995. Weekday vs. weekend ambient ozone concentrations: Discussion and hypotheses with focus on northern California. *J. Air Waste Manage. Assoc.*, 45, 967-972.

Alvarado, M., Lonsdale, C., Yokelson, R., Akagi, S.K., Coe, H., Craven, J., Fischer, E., McMeeking, G., Seinfeld, J., Soni, T., 2015. Investigating the links between ozone and organic aerosol chemistry in a biomass burning plume from a prescribed fire in California chaparral. *Atmos. Chem. Phys.*, 15, 6667–6688.

Atkinson-Palombo, C.M., Miller, J.A., and Balling, R.C. Jr., 2006. Quantifying the ozone "weekend effect" at various locations in Phoenix, Arizona. *Atmos. Environ.*, 40, 7644-7658.

Baylon, P., Jaffe, D., Hall, S., Ullmann, K., Alvarado, M., Lefer, B., 2018. Impact of biomass burning plumes on photolysis rates and ozone formation at the Mount Bachelor observatory. *J. Geophys. Res.*, 123, 2272–2284.

Boian, C., Andrade, M.F., 2012. Characterization of ozone transport among metropolitan regions. *Rev. Bras. Meteorol.*, 27, 229-242.

Carslaw, D.C., 2005. Evidence of an increasing NO2/NOx emissions ratio from road traffic emissions. *Atmos. Environ.*, 39, 4793-4802.

Clapp, L.J., Jenkin, M.E., 2003. Analysis of the relationship between ambient levels of O_3, NO_2 and NO as a function of NOx in the UK. *Atmos. Environ.*, 35, 6391-6405.

675 Crippa, M., Guizzardi, D., Muntean, M., Schaaf, E., Dentener, F., van Aardenne, J.A.,
676 Monni, S., Doering, U., Olivier, J.G.J., Pagliari, V. and Janssens-Maenhout, G., 2018.
677 Gridded Emissions of Air Pollutants for the period 1970–2012 within EDGAR v4.3.2
678 *Earth Syst. Sci. Data*. https://doi.org/10.5194/essd-10-1987-2018.

679 Crutzen, P.J., Andreae, M.O., 1990. Biomass burning in the tropics: Impact on
680 atmospheric chemistry and biogeochemical cycles. *Science*, 250, 1669–1678.

681 Flannigan, M. D., Krawchuk, M. A., de Groot, W. J., Wotton, B. M., Gowman, L. M.,
682 2009. Implications of changing climate for global wildland fire. *Int. J. Wildland Fire*,
683 18, 483–507.

684 Flannigan, M., Cantin, A.S., de Groot, W.J., Wotton, M., Newbery, A., Gowman, L.M.,
685 2013. Global wildland fire season severity in the 21st century. *For. Ecol. Manag.*, 294,
686 54–61.

687 Freitas, S.R., Longo, K.M., Dias, M.A.F.S., Dias, P.L.S., Chatfield, R., Prins, E., Artaxo,
688 P., Grell, G.A., Recuero, F.S., 2005. Monitoring the transport of biomass burning
689 emissions in South America. *Environ. Fluid Mech.*, 5, 135–167.

690 Gandhi, O., Oshiro, A.H., Costa, H.K.M., Santos, E.M., 2017. Energy intensity trend
691 explained for Sao Paulo state. *Renew. Sust. Energ. Rev*., 77, 1046-1054.

692 Governo do Estado de São Paulo, 2019. (http://www.saopauloglobal.sp.gov.br/) (Last
693 accessed 12 February 2019).

694 Grange, S.K., Lewis, A.C., Moller, S.J., Carslaw, D.C., 2017. Lower vehicular primary
695 emissions of NO_2 in Europe than assumed in policy projections. *Nat. Geosci.*, 10, 914-
696 918.

697 Hair, J. F , Tatham, R. L., Anderson, R. E., Black, W., 1998. Multivariate Data Analysis.
698 5th ed. Prentice Hall International, London.

699 Heuss, J.M., Kahlbaum, D.F., Wolff, G.T., 2003. Weekday/Weekend ozone differences:
700 What can we learn from them? *J. Air Waste Manage. Assoc.*, 53, 772-788.

701 INPE, 2018. National Institute for Space Research. Portal for the monitoring of vegetation
702 fires. Available at http://www.inpe.br/queimadas. Last accessed October 21, 2018.

703 INMET, 2018. Instituto Nacional de Meteorologia. Normais Climatológicas do Brasil
704 1981-2010. Available at http://www.inmet.gov.br. Last accessed on April 04, 2019.

705 Jenkin, M.E., Clemitshaw, K.C., 2000. Ozone and other secondary photochemical
706 pollutants: chemical processes governing their formation in the planetary boundary
707 layer. *Atmos. Environ.*, 34, 2499–2527.

708 Jerrett, M., Burnett, R.T., Pope, C.A., Ito, K., Thurston, G., Krewski, D., Shi, Y.L., Calle,
709 E., Thun, M., 2009. Long-term ozone exposure and mortality. *N. Engl. J. Med.*, 360,
710 1085-1095.

711 Junge, C.E., 1962. Global ozone budget and exchange between stratosphere and
712 troposphere. *Tellus*, 4, 363-377.

713 Kalkstein, L. S., Corrigan, P., 1986. A synoptic climatological approach for geographical
714 analysis: Assessment of sulfur dioxide concentrations. *Ann. Assoc. Amer. Geo.*, 76,
715 381-395.

716 Krawchuk, M.A., Moritz, M.A., Parisien, M.-A., Van Dorn, J., Hayhoe, K., 2009: Global
717 pyrogeography: the current and future distribution of wildfire. *PLoS ONE*, 4(4),
718 DOI:10.1371/journal.pone.0005102.

719 Krecl, P., Targino, A.C., Wiese, L., Ketzel, M., 2016. Screening of short-lived climate
720 pollutants in a street canyon in a mid-sized city in Brazil. *Atmos. Poll. Res.*, 7, 1022-
721 1036.

722 Levy, R.C., Remer, L.A., Mattoo, S., Vermote, E.F., Kaufman, Y J., 2007. Second-
723 generation operational algorithm: Retrieval of aerosol properties over land from
724 inversion of Moderate Resolution Imaging Spectroradiometer spectral reflectance. *J.*
725 *Geophys. Res. Atmos*., 112, D13211, doi:10.1029/2006JD007811.
726 Levy, R.C., Mattoo, S., Munchak, L.A., Remer, L.A., Sayer A.M. and co-authors, 2013.
727 The Collection 6 MODIS aerosol products over land and ocean. *Atmos. Meas. Tech*.,
728 6, 2989-3034.
729 Lin, Y. C., Lin, C. Y., Lin, P. H., Engling, G., Lin, Y. C., Lan, Y. Y., Chang, C. W. J.,
730 Kuo, T. H., Hsu, W. T., Ting, C. C., 2013. Influence of Southeast Asian biomass
731 burning on ozone and carbon monoxide over subtropical Taiwan, *Atmos. Environ*., 64,
732 358-365.

733 Lopes, F.J.S., Mariano, G.L., Landulfo, E., Mariano, E.V.C., 2012. Impacts of biomass
734 burning in the atmosphere of the southeastern region of Brazil using remote sensing
735 systems. Atmospheric Aerosols, IntechOpen, DOI: 10.5772/50406.

736 Lyapina, O., Schultz, M.G., Hense, A., 2016. Cluster analysis of European surface ozone
737 observations for evaluation of MACC reanalysis data. *Atmos. Chem. Phys*., 16, 6863–
738 6881.

739 Mazzeo, N.A., Venegas, L.E., Choren, H., 2005. Analysis of NO, NO2, O3 and NOx
740 concentrations measured at a green area of Buenos Aires City during wintertime.
741 *Atmos. Environ.*, 39, 3055–3068.

742 McClure, C.D., Jaffe, D.A., 2018a. Investigation of high ozone events due to wildfire
743 smoke in an urban area. *Atmos. Environ.*, 194, 146-157.

744 McClure, C.D., Jaffe, D.A., 2018b. US particulate matter air quality improves except in
745 wildfire-prone areas. *PNAS*, 115, 7901–7906.

746 Monks, P.S., Archibald, A.T., Colette, A., Cooper, O., Coyle, M., Derwent, R., Fowler,
747 D., Granier, C., Law, K. S., Mills, G. E., Stevenson, D.S., Tarasova, O., Thouret, V.,
748 von Schneidemesser, E., Sommariva, R., Wild, O., and Williams, M.L., 2015.
749 Tropospheric ozone and its precursors from the urban to the global scale from air
750 quality to short-lived climate forcer. *Atmos. Chem. Phys.*, 15, 8889–8973.

751 Notario, A., Bravo, I., Adame, J.A., Díaz-de-Mera, Y., Aranda, A., Rodríguez, A.,
752 Rodríguez, D., 2012. Analysis of NO, NO_2, NOx, O_3 and oxidant ($OX=O_3+NO_2$)
753 levels measured in a metropolitan area in the southwest of Iberian Peninsula. *Atmos.*
754 *Res.*, 104, 217–226.

755 Oliveira, A.M., Mariano, G.L., Alonso, M.F., Mariano, E.V.C., 2016. Analysis of
756 incoming biomass burning aerosol plumes over southern Brazil. *Atmos. Sci. Let.*, DOI:
757 doi.org/10.1002/asl.689.

758 Pancholi, P., Kumar, A., Bikundia, D.S., Chourasiya, S., 2018. An observation of
759 seasonal and diurnal behavior of O3-NOx relationships and local/regional oxidant (OX
760 = O_3 + NO_2) levels at a semi-arid urban site of western India. *Sust. Environ. Res.*, 28,
761 79-89.

762 Pereira, G.M., Teinilä, K., Custódio, D., Santos, A.G., Xian, H., Hillamo, R., Alves, C.
763 A., Andrade, J.B., Rocha, G.O., Kumar, P., Balasubramanian, R., Andrade, M.F.,
764 Vasconcellos, P.C., 2017. Particulate pollutants in the Brazilian city of São Paulo: 1-
765 year investigation for the chemical composition and source apportionment. Atmos.
766 Chem. Phy., 17, 11943-11969.

767 Pivello, V.R., 2011. The use of fire in the Cerrado and Amazon rainforests of Brazil: Past
768 and present. *Fire Ecol.*, 7, 24-39.

769 Pudasainee, D., Sapkota, B., Shrestha, M.L., Kaga, A., Kondo, A., Inoue, Y., 2006:
770 Ground level ozone concentrations and its association with NOx and meteorological
771 parameters in Kathmandu valley, Nepal. *Atmos. Environ.*, 40, 8081-8087.

772 Querol, X., Alastuey, A., Orio, A., Pallares, M., Reina, F., Dieguez, J. J., Mantilla, E.,
773 Escudero, M., Alonso, L., Gangoiti, G., Millán, M., 2016. On the origin of the highest
774 ozone episodes in Spain. *Sci. Total Environ*., 572, 379–389.

775 Reinhardt, T.E., Ottmar, R.D., Castilla, C., 2001. Smoke impacts from agricultural
776 burning in a rural Brazilian town. *J. Air Waste Manage. Assoc.*, 51, 443-450.

777 Riaño, D., Ruiz, J.A.M., Isidoro, D., Ustin, S.L., 2007. Spatial and temporal patterns of
778 burned area at global scale between 1981–2000 using NOAA-NASA Pathfinder. *Glob.*
779 *Change Biol.*, 13, 40-50.

780 Rosário, N. E., Longo, K. M., Freitas, S. R., Yamasoe, M. A., and Fonseca, R. M., 2013.
781 Modeling the South American regional smoke plume: aerosol optical depth variability
782 and Surface shortwave flux perturbation. *Atmos. Chem. Phys*, 13, 2923-2938.

783 Rousseeuw, P.J., 1987. Silhouettes: A graphical aid to the interpretation and validation of
784 cluster analysis. *Comput. Appl. Math.*, 20, 53-65.

785 Sarangi, T., Naja, M., Ojha, N., Kumar, R., Lal, S., Venkataramani, S., Kumar, A., Sagar,
786 R. and Chandola, H. C., 2014. First simultaneous measurements of ozone, CO, and
787 NOy at a high-altitude regional representative site in the central Himalayas, J.
788 Geophys. Res. Atmos., 119, 1592–1611, doi:10.1002/2013JD020631.

789 Sillanpää, M, Saarikoski, S., Hillamo, R., Pennanen, A., Makkonen, U., Spolnik, Z., Van
790 Grieken, R., Koskentalo, T., Salonen, R.O., 2005. Chemical composition, mass size

791 distribution and source analysis of long-range transported wildfire smokes in Helsinki.
792 *Sci. Total Environ*., 350, 119-135.

793 Škerlak, B., Sprenger, M., Wernli, H., 2014. A global climatology of stratosphere-
794 troposphere exchange using the ERA-Interim data set from 1979 to 2011. *Atmos.*
795 *Chem. Phys.*, 14, 913-937.

796 Stein, A.F., Draxler, R.R, Rolph, G.D., Stunder, B.J.B., Cohen, M.D., and Ngan, F., 2015.
797 NOAA's HYSPLIT atmospheric transport and dispersion modeling system, *Bull.*
798 *Amer. Meteor. Soc*., 96, 2059-2077.

799 Targino, A.C., Krecl, P., 2016. Local and regional contributions to black carbon aerosols
800 in a mid-sized city in southern Brazil. *Aeros. Air Qual. Res.*, 16, 125-137.

801 Targino, A. C., Krecl, P., Johansson, C., Swietlicki, E., Massling, A., Coraiola, G. C.,
802 Lihavainen, H., 2013. Deterioration of air quality across Sweden due to transboundary
803 agricultural burning emissions. *Boreal Environ. Res.*, 18, 19-36.

804 Ten Hoeve, J.E., Remer, L.A., Correia, A.L., Jacobson, M.Z., 2012. Recent shift from
805 forest to savanna burning in the Amazon Basin observed by satellite. *Environ. Res.*
806 *Lett.*, 7, 1-8.

807 Torres-Jardon, R., and Keener, T.C., 2006. Evaluation of ozone-nitrogen oxides-volatile
808 organic compound sensitivity of Cincinnati, Ohio. *JAWMA*, 56, 322-333.
809 Vukovich, F.M., 2000. The spatial variation of the weekday/weekend differences in the
810 Baltimore area. *J. Air Waste Manage. Assoc.*, 50, 2067-2072.

811 Wentworth, G.R, Aklilu, Y., Landis, M.S., Hsu, Y.-M., 2018. Impacts of a large boreal
812 wildfire on ground level atmospheric concentrations of PAHs, VOCs and ozone.
813 *Atmos. Environ*, 178 19–30.

814 Wevers, M., De Fré, R., Desmedt, M., 2004. Effect of backyard burning on dioxin
815 deposition and air concentrations. *Chemos.*, 54, 1351–1356.

816 Wilks, D. S., 2011. Statistical methods in the atmospheric sciences (3rd ed.). Oxford ;
817 Waltham, MA: Academic Press.

818 Witham C., Manning A., 2007. Impacts of Russian biomass burning on UK air quality.
819 *Atmos. Environ.*, 41, 8075-8090.

820 Zhou, Y., Luo, B., Li, J., Hao, Y., Yang, W., Shi, F., Chen, Y., Simayi, M., Xie, S., 2019.
821 Characteristics of six criteria air pollutants before, during, and after a severe air
822 pollution episode caused by biomass burning in the southern Sichuan Basin, China.
823 *Atmos. Environ.*, 34, DOI:doi.org/10.1016/j.atmosenv.2019.116840.

824 Ziemke, J.R., Chandra, S., Labow, G.J., Bhartia, P.K., Froidevaux, L., Witte, J.C., 2011.
825 A global climatology of tropospheric and stratospheric ozone derived from Aura OMI
826 and MLS measurements. *Atmos. Chem. Phys*., 11, 9237–9251.